POLITECNICO DI TORINO
Repository ISTITUZIONALE

Active electrode isolation for advanced plasma actuators

(Article begins on next page)

27 September 2024

Active electrode isolation for advanced plasma actuators

J. Serpieri†, M. T. Hehner, & J. Kriegseis

Institute of Fluid Mechanics, Karlsruhe Institute of Technology,
Kaiserstr. 10, 76131, Karlsruhe, Germany

Abstract

A novel concept for actively isolating neighbouring electrodes of multi-electrodes plasma actuators for flow control is presented. For these actuators, such as the phased-array actuators (e.g. Corke & Matlis 2000) or the oscillating-wall ones (e.g. Choi *et al.* 2011), at different time instants, different sets of electrodes are operated; meanwhile the not-operated electrodes are floating grounds for the circuit. The proposed concept consists of splitting the amplitude of the voltage signals supplied to the operated electrodes and needed to generate the plasma discharge in a baseline continuous signal, below the voltage breakdown, and a time-modulated component.

The proposed operation reduces the voltage difference between operated and not-operated neighbouring electrodes. Therefore, related detrimental interactions, such as parasitic discharges, are prevented. Moreover, its implementation does not require extra energy expenditures. Two proof-of-concept experiments are performed and presented showing the proposed operation mode effective and efficient.

1. Contest and motivation

Active flow control is a modern branch of fluid dynamics, which flourished in the last decades (Bushnell 2003). The flow is forced to scope-oriented patterns by means of active devices i.e. devices that spend energy when operated (Cattafesta & Sheplak 2011).

Plasma actuators (PA) are flow actuators that gained major attention in the last decade (Moreau 2007; Corke *et al.* 2010; Kriegseis *et al.* 2016). Several types of PAs have been developed as the corona-discharge (e.g. Velkoff & Ketcham 1968; Yabe *et al.* 1978), the dielectric-barrier discharge (DBD) (e.g. Roth *et al.* 1998) including those whose discharge operates in the nanosecond range (e.g. Correale *et al.* 2015) and the synthetic spark-jet actuators (e.g. Cybyk *et al.* 2004). All the mentioned devices feature high-voltage (HV) electrodes and low-voltage/grounded electrodes between which a strong electric field establishes capable of altering the electric state of the fluid molecules (molecular vibration, ionization, recombination). According to the chosen technology, PAs introduce energy or momentum in the surrounding fluid. Moreover, they can be operated as unsteady forcing devices whose frequency band is extremely broad thus overcoming the limits of mechanic/pneumatic actuators. DBD PAs work on the principle of local, partial ionization of the operated-fluid molecules and consequential acceleration, by Coulomb force (e.g. Moreau 2007), of the electrically-charged particles and, by molecular collision, of the fluid neutral molecules along the electrical-field direction. Accordingly, they introduce a localized, (mainly) wall-aligned body force in the operated fluid causing jets of velocity up to 7 m/s (Forte *et al.* 2007).

† jacopo.serpieri@me.com (corresponding author)

Advanced PAs can perform convoluted actuation patterns where the flow is actuated at different positions at different time instants. They can do so by deploying different sets of electrodes that are operated at different moments in time. An example of these actuators are the phased-array actuators (Corke & Matlis 2000) that have been deployed for a variety of applications as the control of flow separation (e.g. Hultgren & Ashpis 2018) or the control of the friction drag caused by turbulent flows (e.g. Choi *et al.* 2011; Whalley & Choi 2014). Another example, still aiming at turbulent flow drag reduction, are those actuators that create a flow layer at the wall that periodically inverts direction thus mimicking the oscillating-wall forcing (e.g. Choi *et al.* 2011; Mahfoze & Laizet 2017; Hehner *et al.* 2019), which proved effective in reducing the drag exerted by turbulent flows. Notwithstanding the actuation strategy and the actuator design, all these advanced PAs feature several HV electrodes narrowly spaced between each other whose operation occurs at discrete phases of the given actuation cycle. Because of this, at a specific time instant, neighboring HV electrodes might feature large potential differences leading to undesired discharge between them despite the isolation barrier usually installed among the electrodes. These parasitic discharges lower the intensity of the desired discharges and reduce the PA efficiency and lifetime as they appear at undesired regions of the actuator.

The sliding discharge concept was proposed (e.g. Arad *et al.* 1987; Louste *et al.* 2005) as a way of reducing the potential negative effect of the high intensity plasma streamers peculiar of the dielectric barrier (DB) discharge. The concept hereby introduced, however, does not refer to this configuration and neither aims at the same goal.

This document introduces a novel approach to actively isolate HV electrodes of advanced PAs. We named it: active electrode isolation (AEI). This idea has been conceived, and will be presented, for the isolation of electrodes for DBD PAs. Nonetheless, its application could be extended to other actuators (see the DC-pulsed actuator of Thomas *et al.* 2019, for instance), designs and applications where there is the need to improve the isolation of HV electrodes.

2. Active electrode isolation

To introduce the AEI concept, let's consider a DBD PA featuring several HV electrodes each of which can be operated independently. To do so, the HV electrodes need a HV signal of amplitude V. The latter needs to be equal or larger than the so-called breakdown voltage $V*$ at which a strong electric field in the actuator proximity sets and locally exceeds the break-down field strength of the operated fluid. The input voltage signal for a generic i-th electrode is modulated in time with a step function $f_i(t, \gamma)$ whose possible values are comprised in the [0, 1] interval and where t is time and γ is the duty cycle. For a phased-array actuator, a reference duty cycle ($\gamma*$) can be defined by $\gamma* = 100 \%/N$, where N is the number of discrete phases of the whole actuation cycle and thus of the related time-specific electrode(s) sets. Therefore, for $\gamma = \gamma*$, when one of the HV electrode(s) sets is operated, the others are not.

The considered example relates to alternate-current (AC) DBD PA whose inherent working principle relies on a supplied alternating voltage signal harmonically oscillating in time (Corke *et al.* 2010). The plasma AC frequency inherent to a single discharge cycle (unlike the actuation cycle previously mentioned) is considered equal for all HV electrodes and is referred to as g^{AC}. The latter is a function of time but, since the frequency of this function is usually much larger (in the kilo-Hertz range) than the peculiar modulation frequencies for phased-array actuators (10 Hz $\leq f_i \leq 10^2$ Hz), we can ignore to explicitly show this time dependency for the sake of a clearer discussion.
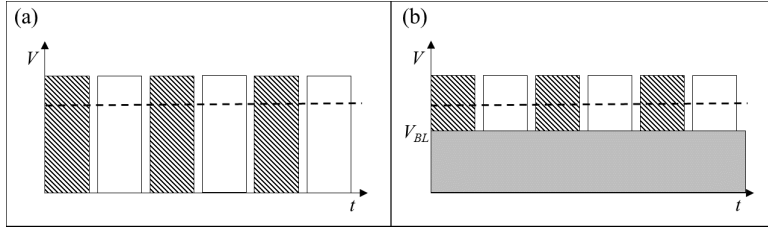
Figure 1: (a) Schematics of an example of voltage-amplitude signals ($f_i(t, \gamma)V$) for a two-electrodes phased-array PA where the dashed line represents the breakdown voltage $V*$ for the considered PA and fluid. (b) Equivalent voltage-amplitude signals ($V_{BL} + f_i(t, \gamma)\Delta V$) according to the AEI concept.

Accordingly, the i-th electrode would receive a voltage signal that can be expressed as: $E_i(t) = g^{AC}f_i(t, \gamma)V$, with $V \geq V*$. In the schematics of figure 1(a), the $f_i(t, \gamma)V$ signals, for an exemplary two-electrodes phased-array PA, are shown: the two f_i functions are the same but shifted in phase and the chosen duty cycle is $\gamma < \gamma* = 50$ %. I.e., at every time instant, either only one electrode (coded with a specific hatching in figure 1) is supplied with a voltage signal whose amplitude exceeds the breakdown voltage (indicated with the dashed line) needed to generate plasma discharge for the specific actuator and fluid or no electrodes are operated. At the time instants at which one electrode is operated, the neighboring electrodes are not supplied with HV signals. Consequently, these behave as floating grounds of the circuit. As such, the voltage difference between them and the operated HV electrode can be comparable with the one between the operated HV electrode and the grounded electrode(s). Accordingly, the intensity of the electric field peculiar of these two possible circuits can be similar with the discriminant parameters guiding the discharge direction being the electrodes isolation and their mutual distance. The possibility of modifying these two parameters to avoid the parasitic discharges among the HV electrodes can be, nonetheless, limited.

   The AEI approach consists of reducing the electric field among time-lagged HV electrodes by directly reducing the potential difference among them. This is done by splitting the voltage amplitude supplied to the HV electrodes in a baseline voltage of amplitude V_{BL}, which is below the breakdown voltage amplitude, and an extra voltage signal of amplitude ΔV. When the HV electrodes receive a voltage signal of amplitude $V = V_{BL} + \Delta V \geq V*$, plasma discharge is generated between the powered and the grounded electrodes. According to the AEI concept, all the HV electrodes are continuously supplied with $g^{AC}V_{BL}$. Therefore, this is to be considered as a voltage offset not consuming any power (besides the power- and HV- suppliers' efficiency losses) being below the breakdown voltage. Instead, the electrode-specific time modulation is left to the signal $g^{AC}f_i(t, \gamma)\Delta V$. By doing so, the maximum voltage-amplitude difference between the time-specific ($\tilde{t}$) operated i-th electrode(s) ($f_i(\tilde{t}, \gamma*) = 1$) and the neighbouring passive electrodes ($f_{j=i}(\tilde{t}, \gamma*) = 0$), including the respective connections, would be ΔV. The latter value is chosen low enough to avoid discharges for the given fluid and PA embodiment. This scenario is shown in the schematics of figure 1(b). Following the AEI approach, the i-th HV electrode would eventually receive a voltage signal that can be expressed as: $E_i^{AEI}(t) = g^{AC}[V_{BL} + f_i(t, \gamma)\Delta V]$.

   The implementation of the proposed approach requires the possibility to modulate the supplied voltage between the values [$V_{BL}, V_{BL} + \Delta V$]. This could be done with a specific electronic circuit whose description goes beyond the scope of this document. As,

introduced, besides the efficiency loss of the electronics equipment, adoption of the AEI operation mode comes without further energy expenditures. The AEI concept considers the electrodes of advanced PAs where the supplied HV signal are modulated in time and can be directly considered for different types of PAs as well as for PAs with more HV electrodes than for the example considered in figure 1.

3. Proof of concept

As a proof of the proposed concept, laboratory experiments were conducted. The setup for the tests is introduced in the following section. The expected discharge scenarios are qualitatively outlined in section 3.2. Particularly, the AEI concept is adopted to cancel parasitic discharges of corona type (section 3.3), and parasitic DB discharges (section 3.4), occurring between two neighbouring HV electrodes.

3.1. Setup

Two identical PAs were manufactured. These will be referred to as actuator A and B, respectively. The exposed electrodes were made of 15 mm wide stripes of 35 μm thick copper tape while the encapsulated electrodes were made of 5 mm wide copper-tape stripes. The dielectric material was a ceramic Al_2O_3 plate, 0.68 mm thick; whereas, insulation of the encapsulated electrodes was provided by means of multiple layers of 70 μm thick polyimide (*Kapton®*) tape. The choice of the dielectric was based on the considerations that polymer-based dielectrics might not withstand for long the thermo-mechanical stresses caused by corona-type discharges.

The two actuators were placed such that the edges of the respective exposed electrode were parallel to and distant 0.5 mm from each other. Note that the considered setup is arbitrary as it aims at demonstrating the proposed concept; the conclusions that will be drawn are, therefore, not specific for the considered application. A schematic showing the considered setup is shown in figures 2(a) and 2(b).

Each of the two exposed electrodes was connected to a HV supplier (*GBS Elektronik GmbH Minipuls 6*); whereas, the encapsulated electrodes were connected to the ground. Each of the HV suppliers was fed with the same AC signal (g^{AC}): a square wave with frequency of 15 kHz, supplied by a *DSO-X 2004A* oscilloscope from *Agilent Technologies*. This oscilloscope was also used to monitor the input signals. The two HV suppliers were operated by means of two *VOLTCRAFT VLP-1405 PRO* laboratory power supply units. The output voltage of one of these power supplies, connected to the HV supplier operating actuator A, was remotely adjusted by means of a control signal as already done for the sake of performance-control by Kriegseis *et al.* (2013). The control signal was a 1 Hz square wave generated by a *National Instruments* board operated by a *Labview* script. The square wave was offset with respect to the ground voltage (V_{GR}) such to oscillate between a maximum value of 2.3 V and a minimum one, coinciding to the value of V_{GR} or to an arbitrary ($> V_{GR}$) value. Accordingly, both the actuator-A power- and HV-supplier output signals would oscillate between a maximum value (set to be larger than the breakdown voltage) and either the V_{GR} value (for reference standard operation) or a given $> V_{GR}$ value (for AEI operation). The actuator B and its related hardware were either not operated (reference case) or set at a constant amplitude corresponding to the low-voltage phase of the input signal of actuator A. Namely, this constant amplitude would correspond to the V_{BL} offset.

It is furthermore worth to mention that the two actuators can be considered to be representative of part of two actuators used by Choi *et al.* (2011) for the introduction in a turbulent flow of oscillating crossflow-directed flow-motions with the simplification that
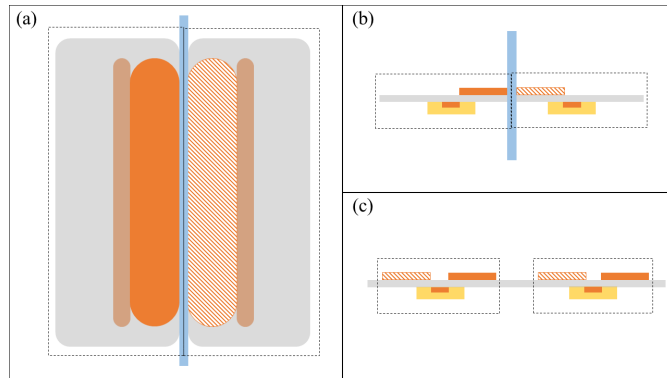
Figure 2: Schematics (not to scale) of the considered setup: (a) top view, (b) side view. The two actuators are shown with the black dashed boxes. The grey shapes represent the ceramic dielectric plates; the light orange shapes (full and dashed) the exposed electrodes; the dark orange shapes the encapsulated electrodes; the yellow shapes the insulating layer and the light-blue shape the void gap or the PET dielectric between the two actuators. (c) Schematics (not to scale) of the adopted actuators assembled according to the layout considered by Choi *et al.* (2011).

only one exposed electrode per actuator was here considered. The considered actuators, when assembled in the layout studied by Choi *et al.* (2011), are shown in figure 2(c) for comparison purposes. The two differently-colored HV electrodes for the application considered by Choi *et al.* (2011) are operated in counter-phase with respect to each other.

As a further simplification, only one actuator (A) was modulated in time. Nonetheless, during the high-voltage phases, parasitic discharges would occur between the exposed electrodes of actuator A and B with the latter being a floating ground for the circuit. These discharges would be of corona type when the space between the HV electrodes was left void. When, instead, a 0.5 mm PET foil was placed, orthogonal to the actuators planes, in the gap between the two actuators (see figure 2), it would feature as a dielectric barrier between anode and cathode thus leading to DB parasitic discharges between the exposed electrodes.

The conclusions drawn for the reduced "oscillating-wall" actuators here tested, i.e. where only the phase corresponding to the forcing along one direction is considered, are directly translated to full Choi *et al.* (2011) actuators given the symmetry of the presented setup. Namely, the actuator A/B can correspond indifferently to the fully-/shaded- colored electrodes of figure 2. It shall be mentioned that, for the considered setup, the gap between the two actuators was here much reduced to dramatize the undesired interference. Nevertheless, parasitic discharges could also take place between the two HV electrodes (full and dashed) pertaining to the same actuator of the Choi *et al.* (2011) actuator configuration. Moreover, faster flows or different applications (see e.g. Hultgren & Ashpis 2018) might demand for PA designs featuring more-narrowly-spaced HV electrodes. Finally, different actuator types (e.g. the DC-pulsed actuator introduced by Thomas *et al.* 2019) might introduce even larger-intensity electric fields, potentially suffering from parasitic discharges even for considerable electrodes' spacing.

The HV signals V_A and V_B supplied to the HV electrodes of both the A and B actuator were recorded by means of one *Pintek HVP-39 pro* HV probe per electrode with de-multiplication factor of 1000:1. The current intensity I_A drawn by actuator A was measured by means of a *Magnelab CT-C1.0* Rogowski coil placed in series between
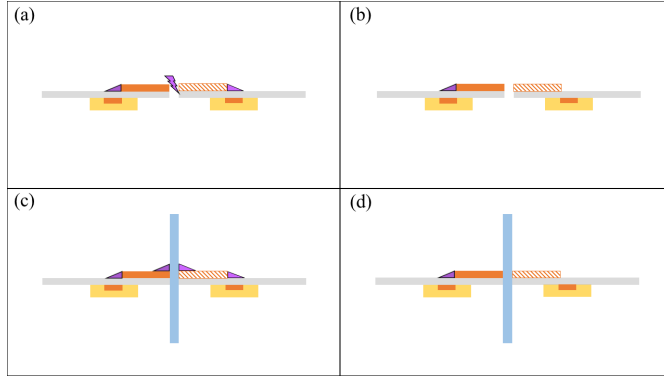
Figure 3: Schematics (not to scale) of the discharges scenario for the tested cases; actuator A: fully colored; actuator B: shaded. (a) case 1; (b) case 2; (c) case 3 and (d) case 4. The purple lighting represents corona discharges; the purple triangle, DB discharges.

the HV supplier and the HV electrode, for both the actuators (cp. Ashpis *et al.* 2017). Finally, the voltage across a 10 nF capacitor mounted in series between the grounded electrode of actuator A and the ground was measured, thus allowing to retrieve the instantaneous charge Q_A (see Kriegseis *et al.* 2011). The resulting four signals (V_A, V_B, I_A, Q_A) were sampled at 100 kHz and digitized by means of a *Pico Technology PicoScope 4424*.

3.2. Tested cases

Four cases were considered. They feature actuators A and B without and with a dielectric layer between them operated in standard modulation and AEI operation. The corresponding settings are summarized in table 1.

The first test case corresponds to a standard modulation of actuator A ($V_A = V_{GR} + f_i(t, \gamma^*)V$). This is the scenario during one of the phases shown in figure 1(a). In this case, the actuator B was not operated and featured as a floating ground for the circuit. The gap between the exposed electrodes was left void and, at every high-amplitude phase of the modulated voltage signal V_A, a series of discharges of corona type occurred between the two exposed electrodes. A schematic of the scenario happening in this case is shown in figure 3(a), where actuator A is considered to be the one with the fully-colored exposed electrode: actuator A induced a DB discharge. Besides, parasitic CD also took place between the two actuators. Further parasitic DB discharge also occurred between the electrodes of actuator B given the high voltage transferred to the exposed electrode of actuator B through the CD.

The second test case considered operation of the same actuators according to the AEI concept. I.e. the low-amplitude phase of the V_A signal did not correspond to the non-operated voltage value, as for the previous case, but to a given level that did not lead to plasma discharge between the electrodes of actuator A. A non-modulated voltage of similar amplitude was supplied also to the HV electrode of actuator B. The parasitic CD between the exposed electrodes was canceled and thus also the DB discharge on actuator B (see figure 3(b)). This voltage amplitude, therefore, corresponds to the baseline voltage V_{BL}. The modulation of the V_A signal between this offset voltage amplitude and the high-voltage one − requested to generate the discharge between the exposed and the encapsulated electrodes − corresponds instead to $f_i(t, \gamma^*)\Delta V$. Briefly, the amplitude of the supplied signals was: $V_B = V_{BL}$ and $V_A = V_{BL} + f_i(t, \gamma^*)\Delta V$.

case	gap between PA A and B	modulation	V_A	V_B
1	void	standard	$V_{GR} + f_i(t, \gamma^*)V$	V_{GR}
2	void	AEI	$V_{BL} + f_i(t, \gamma^*)\Delta V$	V_{BL}
3	PET dielectric	standard	$V_{GR} + f_i(t, \gamma^*)V$	V_{GR}
4	PET dielectric	AEI	$V_{BL} + f_i(t, \gamma^*)\Delta V$	V_{BL}

Table 1: Summary of the tested cases: $V_{BL} \approx 0.5$ kV and $\Delta V \approx 1.5$ kV.

Figure 4: Photography of the CD between the exposed electrodes of actuator A and B for tested case 1.

The third test case represents the standard operation where the parasitic discharges are of the DB type (see figure 3(c)). The PET dielectric foil was therefore placed between the actuators and parasitic DB discharges took place on the two exposed electrodes. A further parasitic DB discharge set between the electrodes of actuator B, although the voltage amplitude on the exposed electrode of actuator B was lower (as it will be shown) than for the parasitic CD case.

For the last test case, by means of the AEI operation, the parasitic DB discharge between the actuators discussed for the third case was canceled and the DB discharge set only between the electrodes of actuator A, as illustrated in figure 3(d).

3.3. AEI for parasitic corona discharges

As introduced, the first case considers standard modulation of actuator A and void gap between the actuators. In these conditions, when operated, actuator A induced a set of CDs on actuator B as it can be seen in the photography of figure 4.

A 10 s time series of the sampled signals is shown for this case in figure 5. It is possible to see the modulation of the HV-electrode voltage signal (V_A) and how this modulation can be appreciated in all the other signals. A filter, built on the V_A signal, was used to differentiate and plot in different colors the high- and low- voltage phases corresponding to all the measured signals. What needs to be emphasized here is the magnitude of the current intensity (I_A), which reaches very large values during the high-voltage phases. These current values are not due to the DB-type discharge between the electrodes of actuator A. Instead, they are attributed to the corona discharge between the exposed electrodes of the two actuators, as outlined in section 3.2. Accordingly, the voltage measured on the exposed electrode of actuator B – despite not actively operated – reached values comparable to the ones measured for the HV electrode of actuator A.

The same hardware was then operated according to the AEI concept setting, for these specific tests: $V_{BL} \approx 0.5$ kV and ΔV 1.5 kV. The modulation of the HV signal supplied to actuator A was now such to correspond to the scenario illustrated in figure 1(b). The corresponding sampled signals are shown in figure 6. For this case, the corona discharge
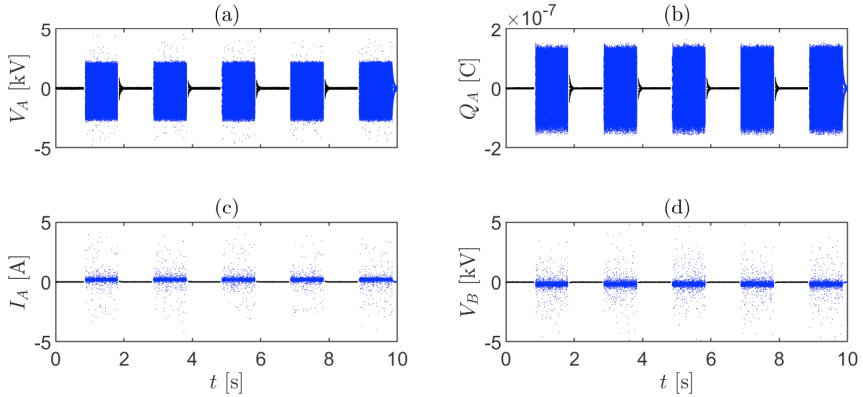
Figure 5: 10 s time traces of V_A (a): high-voltage phase in blue, low-voltage phase in black; and of: Q_A (b), I_A (c) and V_B (d); tested case 1.
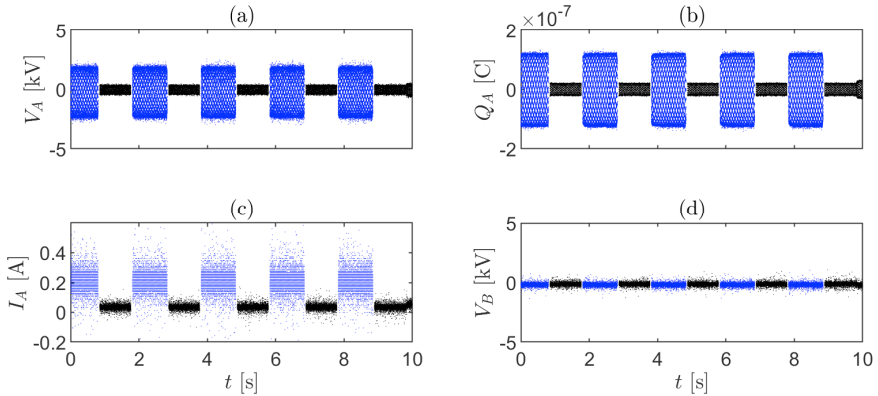

Figure 6: Same caption as for figure 5; tested case 2.

between the exposed electrodes was canceled due to the effectively-reduced potential difference between either electrodes. This was, first of all, visually evident but can be also seen by the much lower amplitude reached, during the high-voltage phase of V_A, by the I_A signal. The highest measured values for this case are about one order of magnitude lower than the ones shown in figure 5 and are peculiar of DB discharges. Another evidence of the AEI efficacy is shown by the voltage signal on the HV electrode of actuator B, which does not suffer from the strong modulation caused by the discharge from the HV electrode of actuator A.

Small differences in amplitude between the voltage supplied to actuator B and the low-phase of the voltage supplied to actuator A are due to the residual mutual interference between the two HV electrodes.

Another diagnostics to inspect the discharge of a DBD PA is plotting the Lissajous curves of the voltage versus the charge across the actuator. Namely, the surface enclosed by the temporal realizations of these two signals corresponds to the power per-cycle consumed by the actuator (see eg. Kriegseis *et al.* 2011). The Lissajous figures of the signals shown in figures 5 and 6 are contrasted in figures 7(a) and 7(b), respectively,
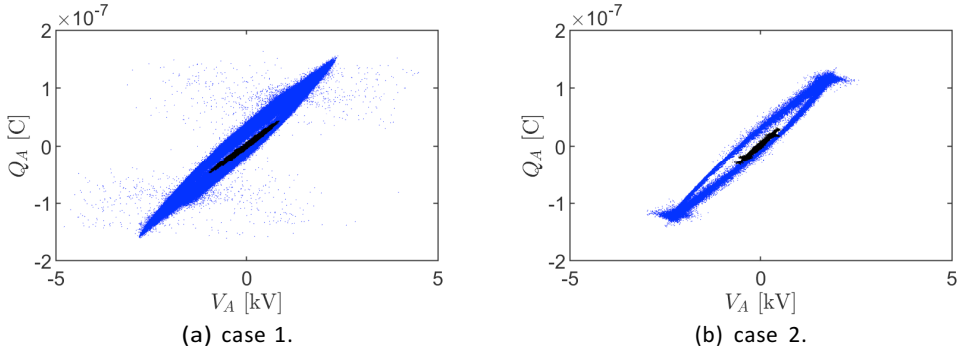
(a) case 1.   (b) case 2.

Figure 7: Lissajous curves of V_A vs Q_A for the signals shown in figure 5 (a) and for the signals shown in figure 6 (b).

using the same color coding for the two phases of the V_A modulation function. It can be seen that, for the reference case, the typical "almond"-shaped Lissajous curve has, for the high-voltage points, a very large scatter of the samples. Furthermore, measured points fill also the region within the curve edges. These effects can be caused by the parasitic corona discharge set between the exposed electrodes of the two actuators scattering the measurement points and lowering the signal-to-noise of the diagnostics. Furthermore, the induced DB discharge on actuator B – whose current intensity was not measured –, influencing V_A but not I_A, could also contribute to this effect.

On the other side, the operation of the actuators according to the AEI concept, retrieves, for the high-voltage phases, a normal DB-discharge curve: so, with more-defined external and internal edges. Furthermore, for the AEI case, the low-voltage phase samples appear similar to those for the standard operation and thus they encircle a very small surface. This corroborates the statement that the AEI operation of the actuators does not come at the price of additional energy expenditures (besides the power- and HV-suppliers' efficiency losses).

3.4. AEI for parasitic DB discharges

The third studied case, reproduces the first one with the only difference being that now the PET foil was installed between the HV electrodes of the two actuators thus modifying the nature of the discharge from the corona to the dielectric barrier type. This was visibly evident during the V_A operated phases. The measured signals are shown in figure 8. The main differences with the corona-discharge case of figure 5 are that the current amplitude I_A does not reach the very high values peculiar of the corona-discharge case. Moreover, the induced voltage on the non-operated actuator B electrode – although still showing some level of modulation – keeps considerably lower values due to the weakened electrical field (compared to case 1) caused by the installation of the dielectric layer between the actuators.

The last case considers the operation of the actuators according to the AEI concept (so with $V_B = V_{BL}$ and $V_A = [V_{BL} + f_i(t, \gamma^*)\Delta V]$) with the same PET foil installed between A and B. The measured signals are shown in figure 9. The voltage signals supplied to the HV electrode of the two actuators are comparable to the ones shown in figure 6 and already discussed. The DB discharge between the HV electrodes of A and B was no more visible for this case. The cancellation of this parasitic discharge can be appreciated less than for the corona discharge case from the sampled signals. Nonetheless, the I_A plot
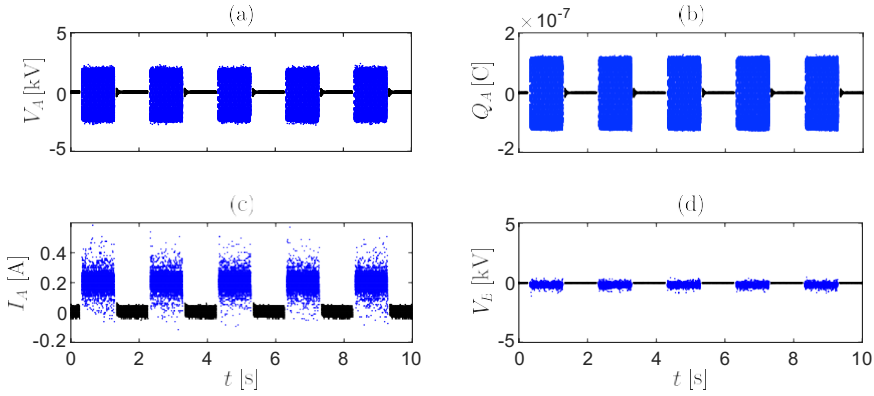
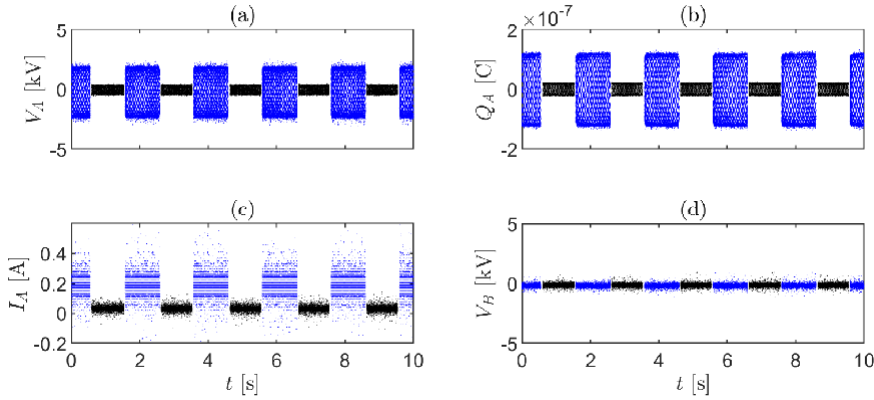Figure 8: Same caption as for figure 5; tested case 3.

Figure 9: Same caption as for figure 5; tested case 4.

appears more faded for this case compared to the case 3 one. This indicates that fewer discharges took place for this scenario. This is likely attributed to the cancellation of the parasitic discharges. This case confirms the possibility of adopting the AEI strategy also for cases where an insulation layer is present between – and, yet, is not sufficient to isolate – neighbouring HV electrodes operated at different time instants as the ones of phased plasma arrays or those adopted for mimicking the oscillating-wall forcing. This type of parasitic discharges surely is less concerning compared to the corona discharges as lower voltages and currents are here at play. Nevertheless, these discharges contribute to the power consumed by the actuator thus lowering its efficiency. Moreover, the insulation serving in this case as a dielectric barrier can be deteriorated by the related plasma species.

4. Concluding remarks and outlook

Advanced flow-control PAs provide spatio-temporally varying flow actuation possibilities. Their design can feature several HV electrodes narrowly spaced and operated at different time instants (see e.g. Corke & Matlis 2000; Wilkinson 2003; Choi *et al.* 2011; Whalley & Choi 2014; Hultgren & Ashpis 2018; Hehner *et al.* 2019). Despite the available distance and the opportune isolation between the electrodes, the electric field that sets

among these HV electrodes can lead to parasitic discharges among them with negative consequences for the actuator efficiency, lifetime and even for the integrity of the model upon which the actuator is mounted.

In this document, we described a novel approach to improve the isolation of neighbouring HV electrodes of advanced PAs by actively reducing the intensity of the electric field setting among the operated HV electrodes and the neighbouring not-operated ones. The approach hereby-introduced is thus named: active electrode isolation (AEI). The proposed strategy implies that the voltage amplitude needed to generate plasma discharge between the HV electrode(s) and the grounded electrode(s) is split in amplitude in two contributions. One is an offset amplitude below the breakdown voltage, which is continuously supplied to all the HV electrodes. The other is an extra amplitude, which is supplied only to the HV electrode(s) that needs, at the considered time instants, to generate plasma discharge. Consequently, the voltage difference between the operated electrode(s) and the neighbouring HV electrode(s) is reduced to a lower level, below the breakdown voltage, successfully preventing plasma discharge between them. The proposed operation can be done by means of the opportune electronic circuit capable of modulating in time the supplied voltage signals.

A proof-of-concept of the proposed approach considering two AC-DBD PAs, whose layout was inspired by the actuators of Choi *et al.* (2011), was presented and showed the capability of preventing the parasitic discharges, whether of corona or dielectric-barrier nature, between neighbouring time-lagged HV electrodes. The proposed concept resulted effective and efficient, not requesting further energy expenditures. It can be, therefore, concluded from the presented proof-of-concept study that the AEI approach might be a valuable operating concept for advanced and/or complex PA arrays. The concept propose here for DBD PAs, like the mentioned phased-array or the "oscillating-wall" actuators, could be considered for other designs or other types of actuators. Finally, a future study could be aimed at assessing the effect of the proposed operation mode on the actuator long-term performance and lifetime as well as at individuating the optimal values of V_{BL} and ΔV for different actuator configurations.

Acknowledgements

REFERENCES

ARAD, B., GAZIT, Y. & LUDMIRSKY, A. 1987 A sliding discharge device for producing cylindrical shock waves. *Journal of Physics D: Applied Physics* **20**, 360–367.

ASHPIS, D.E., LAUN, M.C. & GRIEBELER, E.L. 2017 Progress toward accurate measurement of dielectric barrier discharge plasma actuator power. *AIAA Journal* **55** (7), 2254–2268.

BUSHNELL, D. M. 2003 Aircraft drag reduction—a review. *Proceedings of the I MECH E Part G Journal of Aerospace Engineering* **217** (1), 1–18.

CATTAFESTA, L. N. & SHEPLAK, M. 2011 Actuators for Active Flow Control. *Annu. Rev. Fluid Mech.* **43**, 247–272.

CHOI, K. S., JUKES, T. & WHALLEY, R. 2011 Turbulent boundary-layer control with plasma actuators. *Philosophical Transactions of the Royal Society A: Mathematical, Physical and Engineering Sciences* **369** (1940), 1443–1458.

CORKE, T. C., ENLOE, C. L. & WILKINSON, S. P. 2010 Dielectric barrier discharge plasma actuators for flow control. *Annual Review of Fluid Mechanics* **42**, 505–529.

CORKE, T. C. & MATLIS, E. 2000 Phased plasma arrays for unsteady flow control. *Fluids 2000 Conference and Exhibit* .

CORREALE, G., WINKEL, R. & KOTSONIS, M. 2015 Energy deposition characteristics of nanosecond dielectric barrier discharge plasma actuators: Influence of dielectric material. *Journal of Applied Physics* **118** (8).

CYBYK, B. Z., WILKERSON, J. T. & GROSSMAN, K. R. 2004 Performance characteristics of the sparkjet flow control actuator. *2nd AIAA Flow Control Conference* .

FORTE, M., JOLIBOIS, J., PONS, J., MOREAU, E., TOUCHARD, G. & CAZALENS, M. 2007 Optimization of a dielectric barrier discharge actuator by stationary and non-stationary measurements of the induced flow velocity: Application to airflow control. *Experiments in Fluids* **43**, 917–928.

HEHNER, M. T., GATTI, D. & KRIEGSEIS, J. 2019 Stokes-layer formation under absence of moving parts - A novel oscillatory plasma actuator design for turbulent drag reduction. *Physics of Fluids* **31** (5), 1–6.

HULTGREN, L. S. & ASHPIS, D. E. 2018 Demonstration of separation control using dielectric barrier discharge plasma actuators. *AIAA Journal* **56** (11), 4614–4620.

KRIEGSEIS, J., MÖLLER, B., GRUNDMANN, S. & TROPEA, C. 2011 Capacitance and power consumption quantification of dielectric barrier discharge (dbd) plasma actuators. *Journal of Electrostatics* **69** (4), 302–312.

KRIEGSEIS, J., SCHRÖTER, D., BARCKMANN, K., DUCHMANN, A., TROPEA, C. & GRUNDMANN, S. 2013 Closed-loop performance control of dielectric-barrier-discharge plasma actuators. *AIAA Journal* **51** (4), 961–967.

KRIEGSEIS, J., SIMON, B. & GRUNDMANN, S. 2016 Towards In-Flight Applications? A Review on Dielectric Barrier Discharge-Based Boundary-Layer Control .

LOUSTE, C., ARTANA, G., MOREAU, E. & TOUCHARD, G. 2005 Sliding discharge in air at atmospheric pressure: Electrical properties. *Journal of Electrostatics* **63**, 615–620.

MAHFOZE, O. & LAIZET, S. 2017 Skin-friction drag reduction in a channel flow with streamwise-aligned plasma actuators. *International Journal of Heat and Fluid Flow* **66**, 83–94.

MOREAU, E. 2007 Airflow control by non-thermal plasma actuators. *Journal of Physics D: Applied Physics* **40**, 605–636.

ROTH, J. REECE, SHERMAN, D. M. & WILKINSON, S. P. 1998 Boundary layer flow control with a one atmosphere uniform glow discharge surface plasma. *36th AIAA Aerospace Sciences Meeting and Exhibit* .

THOMAS, F. O., CORKE, T. C., DUONG, A., MIDYA, S. & YATES, K. 2019 Turbulent drag reduction using pulsed-DC plasma actuation. *Journal of Physics D: Applied Physics* **52** (43).

VELKOFF, HENRY R. & KETCHAM, JEFFRY 1968 Effect of an electrostatic field on boundary-layer transition. *AIAA Journal* **6**, 1381–1383.

WHALLEY, R. D. & CHOI, K. S. 2014 Turbulent boundary-layer control with plasma spanwise travelling waves. *Experiments in Fluids* **55** (8).

WILKINSON, S. P. 2003 Investigation of an oscillating surface plasma for turbulent drag reduction. *41st Aerospace Sciences Meeting and Exhibit* .

YABE, AKIRA, MORI, YASUO & HIJIKATA, KUNIO 1978 Ehd study of the corona wind between wire and plate electrodes. *AIAA Journal* **16**, 340–345.